

# Magneto-transport in copper-doped noncentrosymmetric BiTeI

Chang-Ran Wang,<sup>1</sup> Jen-Chuan Tung,<sup>2</sup> R. Sankar,<sup>3</sup> Chia-Tso Hsieh,<sup>1</sup>  
Yung-Yu Chien,<sup>1</sup> Guang-Yu Guo,<sup>2,4</sup> F. C. Chou,<sup>3</sup> and Wei-Li Lee<sup>1,\*</sup>

<sup>1</sup>*Institute of Physics, Academia Sinica, Nankang, Taipei 11529, Taiwan*

<sup>2</sup>*Graduate Institute of Applied Physics, National Chengchi University, Taipei 11605, Taiwan*

<sup>3</sup>*Center for Condensed Matter Sciences, National Taiwan University, Taipei 10617, Taiwan*

<sup>4</sup>*Department of Physics and Center for Theoretical Sciences,  
National Taiwan University, Taipei 10617, Taiwan*

(Dated: July 21, 2018)

BiTeI exhibits large Rashba spin splitting due to its noncentrosymmetric crystal structure. The study of chemical doping effect is important in order to either tune the Fermi level or refine the crystal quality. Here, we report the magneto-transport measurement in high quality BiTeI single crystals with different copper dopings. We found that a small amount of copper doping improves the crystal quality significantly, which is supported by the transport data showing higher Hall mobility and larger amplitude in Shubnikov-de Haas oscillation at low temperature. Two distinct frequencies in Shubnikov-de Haas oscillation were observed giving extremal Fermi surface areas of  $A_S = 9.1 \times 10^{12} \text{ cm}^{-2}$  and  $A_L = 3.47 \times 10^{14} \text{ cm}^{-2}$  with corresponding cyclotron masses  $m_S^* = 0.0353 m_e$  and  $m_L^* = 0.178 m_e$ , respectively. Those results are further compared with relativistic band structure calculations using three reported Te and I refined or calculated positions. Our analysis infers the crucial role of Bi-Te bond length in the observed large bulk Rashba-type spin splitting effect in BiTeI.

PACS numbers:

BiTeI emerges as an intriguing material that shows a large Rashba effect [1–3] and a possible topological phase transition under pressure [4]. Its crystal structure comprises alternating layers of bismuth (Bi), tellurium (Te) and iodine (I) each with trigonal planar lattice as illustrated in Fig. 1(a). It was proposed [5] to constitute a semi-ionic structure along the stacking direction, where (BiTe)<sup>+</sup> layer is positively charged and (Bi-I) layer is ionic. Angle-resolved photo-emission spectroscopy experiments (ARPES) [1, 6] have revealed evidence for the giant Rashba spin splitting, and its bulk nature was further confirmed by bulk-sensitive optical spectroscopy [7] and soft x-ray ARPES [8]. When comparing to band structure calculation, the Te and I coordinations turn out to be crucial parameters that can result in dramatic difference in the calculated band property. There are three different Te and I coordinations reported in the literature: coordination A with Te(2/3,1/3,0.6928) and I(1/3,2/3,0.2510) from the refinement analysis of X-ray experiment [5], as well as coordination B with Te(2/3,1/3,0.7111) and I(1/3,2/3,0.2609)[9], and coordination C with Te(2/3,1/3,0.7482) and I(1/3,2/3,0.3076) [10], from two different theoretical structural determinations using the same band structure method. Regardless of the small variation, only coordination C with a shortest Bi-Te bond length ( $d_{\text{Bi-Te}} = 3.05 \text{ \AA}$ ) gives rise to a giant Rashba spin-splitting in the bulk band with a Rashba parameter  $\alpha_R \cong 5.4 \text{ eV\AA}$  according to our calculations, which may infer a close connection between  $d_{\text{Bi-Te}}$  and its Rashba effect.

In this paper, we show magneto-transport measurement results on high quality  $\text{Cu}_x\text{BiTeI}$  single crystals

with copper (Cu) doping  $x$  up to 0.2. Comparing to earlier works on Shubnikov-de Haas (SdH) oscillations [11, 12], the SdH oscillation in our crystals exhibits two distinct frequencies derived from a large Fermi surface (LFS) and a small Fermi surface (SFS), which is an order of magnitude larger in amplitude at similar temperatures. The corresponding Fermi surface areas and cyclotron masses can then be unambiguously determined and compared to relativistic band structure calculations using three different atomic coordinations A, B and C with progressive reduction in  $d_{\text{Bi-Te(I)}}$ . Our experimental results, including the angular dependence of SdH frequencies, are in good agreement with the calculation using coordination C and thus provide a strong evidence for the bulk nature of the large Rashba spin-splitting effect.

Single crystals of BiTeI were grown by direct mixing of pristine elements of Bi, Te and I with additional room temperature agglomeration procedure [13]. The powder X-ray diffraction patterns of ground BiTeI crystals with Cu content  $x = 0, 0.075$  and  $0.1$  are shown in Fig. 1(b), where the lattice parameters were determined using space group  $P3m1$  to be  $a = b = 4.3421 \text{ \AA}$  and  $c = 6.8835 \text{ \AA}$  for the pristine sample of  $x = 0$ . As  $x$  increases, the lattice expands more along the stacking direction as shown in the inset of Fig. 1(b). The in-plane resistivity  $\rho$  shown in Fig. 1(c) exhibits metallic behavior down to 5 K below which it becomes nearly temperature independent. The carrier density  $n_e$  and Hall mobility  $\mu_H$  were obtained from the Hall effect measurement and shown in the upper inset of Fig. 1(c). It is quite evident that the addition of Cu effectively reduces the electron concentration in BiTeI and improves the carrier mobility by nearly

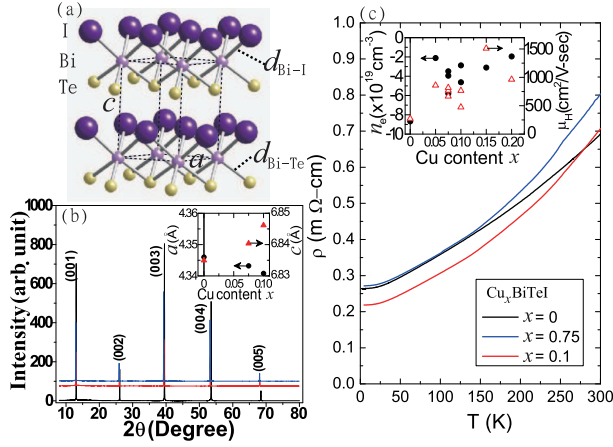


FIG. 1: (color online) (a) An Illustration of the BiTeI crystal structure.  $d_{\text{Bi-Te(I)}}$  is the Bi-Te(I) bond length. (b) shows the powder X-ray diffraction pattern of ground  $\text{Cu}_x\text{BiTeI}$  single crystals with  $x = 0, 0.075$  and  $0.1$ . The inset figure shows the  $x$  dependence on the lattice constants  $a$  and  $c$ . (c) The resistivity  $\rho(T)$  for  $x = 0, 0.075$  and  $0.1$  crystals. The upper inset plots the carrier density  $n_e$  (solid circle) and the corresponding Hall mobility  $\mu_H$  (open triangle) at  $5$  K versus Cu content  $x$ .

an order of magnitude, where SdH oscillation appears with a large amplitude and enables the extraction of the band parameters to be compared with relativistic band calculations.

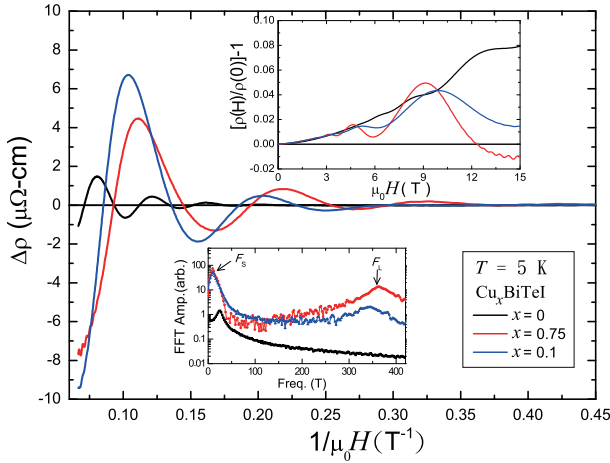


FIG. 2: (color online) The oscillatory component of the resistivity  $\Delta\rho$  as a function of  $1/\mu_0H$  at  $5$  K for  $x = 0, 0.075$  and  $0.1$  crystals. The upper inset shows the magneto-resistance before subtracting the non-oscillatory component of the resistivity. The corresponding FFT spectrum is shown in the lower inset, where two local extremes at  $F_S$  and  $F_L$  can be clearly identified.

The upper inset of the Fig.2 shows the magneto-resistance (MR)  $[\rho(H)/\rho(0)] - 1$  for  $x = 0, 0.075$  and  $0.1$  as a function of magnetic field up to  $15$  T at  $T = 5$  K. It exhibits positive MR and starts to show SdH oscil-

lations above  $3$  T. The pure oscillatory component  $\Delta\rho$  in the resistivity [14] is extracted and plotted as a function of  $1/\mu_0H$  shown in Fig. 2. We remark that the oscillation amplitude is at least 3-fold larger comparing to the undoped for samples with  $x = 0.075$  and  $0.1$  as shown in red- and blue-lines, respectively. By taking the fast Fourier transformation (FFT) of the MR data, two apparent peaks at  $F_S$  and  $F_L$  for  $x = 0.075$  and  $0.1$  were identified in the FFT spectrum shown in the lower inset of Fig. 2, where the suffixes S and L are referred as deriving from a SFS and a LFS, respectively.

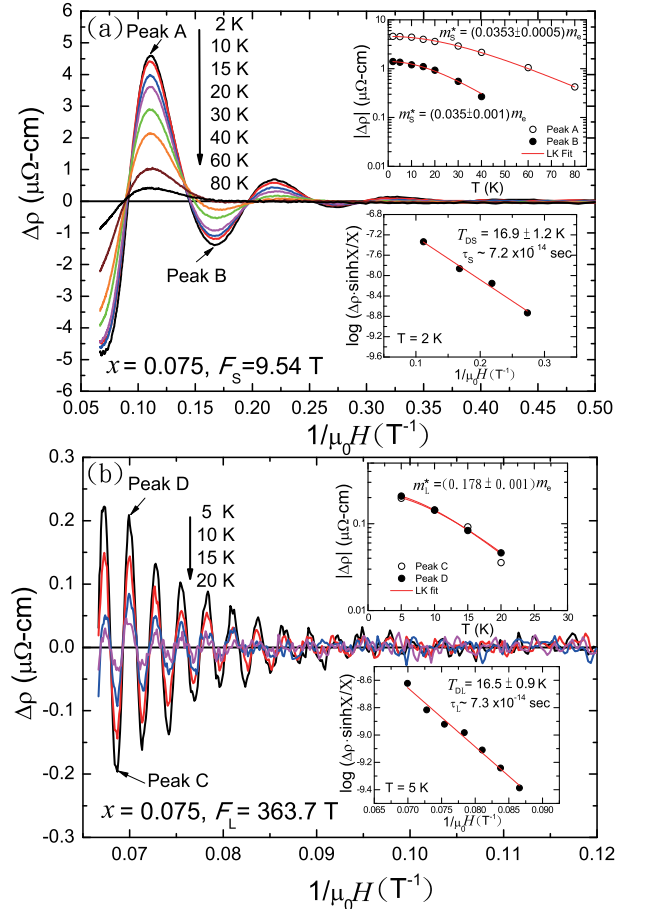


FIG. 3: (color online) (a) SdH oscillations of SFS at 8 different temperatures up to  $80$  K. The temperature dependence of amplitude  $|\Delta\rho|$  at Peak A (open circle) and Peak B (solid circle) are shown in the upper inset. The red lines are fitting curves using LK formula for effective cyclotron mass  $m^*$  determination. The lower inset shows the linear fit to  $\log(\Delta\rho \cdot \sinh X/X)$  at local peaks versus  $1/\mu_0H$ , where the Dingle temperature  $T_D$  can be calculated from the slope. Similarly, (b) shows the SdH oscillations of LFS at 4 different temperatures. The  $m^*$  and  $T_D$  are determined via LK formula fitting as shown in the upper inset and lower inset, respectively.

According to Lifshitz-Kosevich (LK) formalism,  $\Delta\rho$

can be expressed as

$$\frac{\Delta\rho(T, B)}{4\rho_0} = \exp[-X(T, B)] \frac{X(T, B)}{\sinh(X(T, B))}, \quad (1)$$

where  $\rho_0$  is the non-oscillatory component of the zero-field resistivity,  $X(T, B) \equiv 2\pi^2 k_B T m^* / \hbar e B$ ,  $m^*$  is the effective cyclotron mass and  $T_D$  is the Dingle temperature. Figure 3(a) and (b) show the oscillatory component  $\Delta\rho$  as a function of  $1/\mu_0 H$  at different temperatures in  $x = 0.075$  sample arising from SFS and LFS, respectively. In Fig. 3(a), the SdH frequency  $F_S$  equals 9.54 T with oscillation amplitude as large as  $5 \mu\Omega\text{cm}$  at 2 K, where it remains observable with temperature as high as 80 K. By fitting the temperature dependence of  $\Delta\rho$  with LK formula shown in the upper inset in Fig. 3(a), we obtained consistent effective cyclotron masses  $m_S^* = 0.0353 \pm 0.0005 m_e$  and  $0.035 \pm 0.001 m_e$  for peak A and peak B locations, respectively, where  $m_e$  is the electron rest mass. For  $T_{DS}$  determination, we plot  $\log(|\Delta\rho| \cdot \sinh X/X)$  at local extremes as a function of their corresponding  $1/\mu_0 H$  as demonstrated in the lower inset of Fig. 3(a). The data points can be linearly fitted based on LK formula giving a  $T_{DS} = 16.9 \pm 1.2$  K which corresponds to an electron scattering lifetime  $\tau_S \equiv \hbar/2\pi k_B T_{DS} \cong 7.2 \times 10^{-14}$  sec. On the other hand, Fig. 3(b) shows the SdH oscillation arising from LFS giving a  $F_L = 363.7$  T. The effective cyclotron mass  $m_L^*$  equals  $0.178 \pm 0.001 m_e$  from the LK fitting using either peak C or D as shown in the upper inset of Fig. 3(b). The  $T_{DL}$  is about  $16.5 \pm 0.9$  K giving a  $\tau_L \cong 7.3 \times 10^{-14}$  sec. The extremal Fermi surface area  $A_e$  perpendicular to the field direction can be deduced from the SdH oscillation frequency via the Onsager formula  $F = \frac{\hbar}{2\pi e} A_e$ , which gives  $A_S = 9.1 \times 10^{12} \text{ cm}^{-2}$  and  $A_L = 3.47 \times 10^{14} \text{ cm}^{-2}$  for SFS and LFS, respectively.

To gain insight into our magneto-transport experiments, we perform relativistic band structure calculations for BiTeI within the density functional theory with the generalized gradient approximation (GGA)[15] by using the accurate projector augmented-wave (PAW) method, as implemented in the VASP package[16, 17]. All three coordinations A[5], B[9] and C[18] were considered. A large plane-wave cut-off energy of 250 eV was used. The calculated band structures are shown in Fig. 4 where three horizontal dashed lines in black, red and blue denote the Fermi level for electron density  $n_e = 8.7, 5.8$  and  $3.5 (\times 10^{19} \text{ cm}^{-3})$ , respectively, which were set based on the experimental electron densities in crystals of  $x = 0, 0.075$  and  $0.1$ . We remark that large bulk Rashba spin splitting occurs only for coordination C. Using a rigid band assumption, the Cu doping merely decreases the carrier density of the system and hence shifts the Fermi level lower. We found that experimental values of  $F$  and  $m^*$  at three different carrier densities of  $n_e = 3.5, 5.8$  and  $8.7 (\times 10^{19} \text{ cm}^{-3})$  as listed in Table I are much more close to the calculated values using coordination C, which

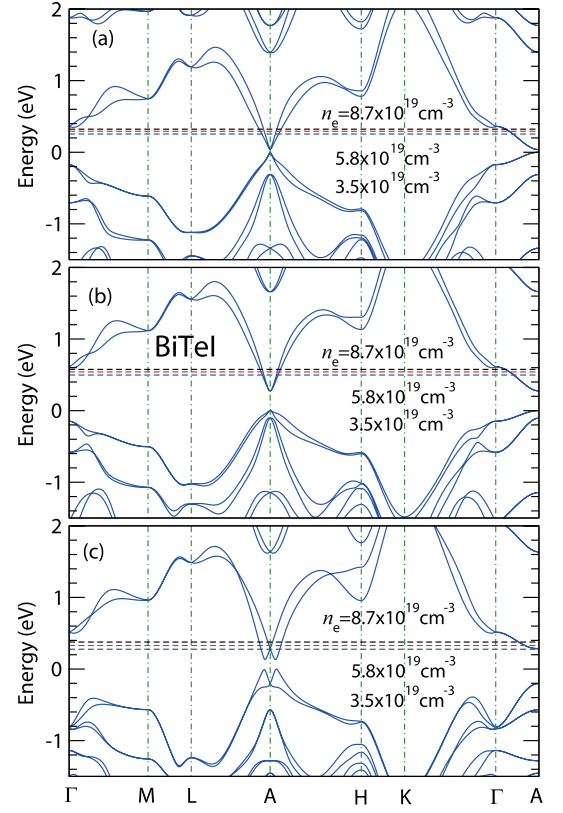


FIG. 4: (color online) Relativistic band structure of BiTeI in the trigonal P3m1 structure using coordination A from Ref. [5] (a) and as well as the theoretically determined coordination B [9] (b) and coordination C [18] (c). The top of the valence band is at 0 eV. The lower, middle and upper dashed horizontal lines denote the Fermi level for electron concentrations  $n_e = 3.5, 5.8$  and  $8.7 (\times 10^{19} \text{ cm}^{-3})$ , respectively.

gives the shortest bond length  $d_{\text{Bi-Te}} = 3.05 \text{ \AA}$ .

We also performed angular dependence of the SdH oscillation for two  $x = 0.075$  crystals in the same batch to further identify the shape of Fermi surface [14]. The normalized SdH frequency  $F_{S(L)}/F_{S(L)}(\theta = 0)$  as a function of field angle  $\theta$  is plotted in Fig. 5(a), where the closed (open) symbols and solid (dashed) lines are experimental data and calculated values for SFS (LFS), respectively. The field angle  $\theta$  is defined as the angle between the stacking direction  $\vec{c}$  and external field as illustrated in the inset cartoon of Fig. 5(a). Even though the SdH frequency differs slightly from sample to sample in the same batch, we remark that the normalized SdH frequency  $F_{S(L)}/F_{S(L)}(\theta = 0)$  remains to follow well with the calculated band using coordination C as shown in the circles and triangles in Fig. 5(a). For more than 4 crystals of  $x = 0.075$  in the same batch we measured,  $F_S(\theta = 0)$  values fall in a range of 3.6 – 9.54 T with corresponding electron density in a range of  $3.5 - 5.8 \times 10^{19} \text{ cm}^{-3}$ . This somewhat large variation in  $F_S(\theta = 0)$  turns out to have no apparent correlation with  $n_e$  [14] and thus

TABLE I: Comparison of calculated SdH frequency  $F(T)$  and effective mass  $m^*(m_e)$  using three different coordinations to experimental data.  $d_{\text{Bi-Te(I)}} (\text{\AA})$  denotes the Bi-Te(I) bond length. Calculated Rashba parameter  $\alpha_R = 0$  for coordinations A and B. For coordination C,  $\alpha_R = 5.46$  (5.35) eV\AA along the AL (AH) direction (see Fig. 4(c)).

$n_e(10^{19} \text{ cm}^{-3})$		3.5		5.8		8.7	
SdH parameters		$F$ (T)	$m^*$ ( $m_e$ )	$F$ (T)	$m^*$ ( $m_e$ )	$F$ (T)	$m^*$ ( $m_e$ )
Coordination A <sup>a</sup>	LFS	175	0.203	247	0.247	317	0.285
	$d_{\text{Bi-Te(I)}} = 3.27$ (3.04) SFS	72.7	0.077	99.5	0.091	125	0.104
Coordination B <sup>b</sup>	LFS	151	0.143	210	0.173	268	0.2
	$d_{\text{Bi-Te(I)}} = 3.19$ (3.08) SFS	104	0.088	140	0.101	173	0.114
Coordination C <sup>c</sup>	LFS	319	0.167	397	0.178	475	0.196
	$d_{\text{Bi-Te(I)}} = 3.05$ (3.30) SFS	0	-	4.4	0.023	18.8	0.047
Experimental data	LFS	339	0.186	364	0.178	-	-
	SFS	9.2	0.037	9.5	0.035	24.8	0.068

<sup>a</sup>Te(2/3,1/3,0.6928), I(1/3,2/3,0.2510)[5]

<sup>b</sup>Te(2/3,1/3,0.7111), I(1/3,2/3,0.2609)[9]

<sup>c</sup>Te(2/3,1/3,0.7458), I(1/3,2/3,0.3133)[18]

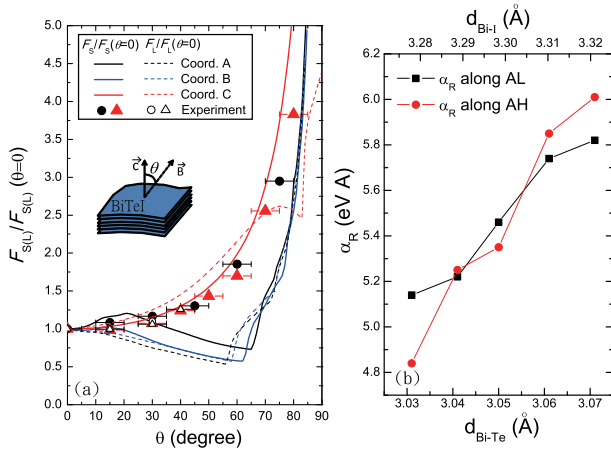


FIG. 5: (color online) (a) Relative SdH oscillation frequency  $F_{S(L)}/F_{S(L)}(\theta = 0)$  as a function of  $\theta$  for two  $x = 0.075$  crystals are shown as solid (open) symbols.  $\theta$  is defined as the angle between the BiTeI stacking direction  $\vec{c}$  and magnetic field direction  $\vec{B}$  as illustrated in the inset cartoon. The solid (dashed) lines are the calculated  $F_{S(L)}/F_{S(L)}(\theta = 0)$  using coordination A, B and C. The experimental data points agree well with the calculated curves using coordination C within the error. (b) Calculated Rashba parameter  $\alpha_R$  versus given Bi-Te bond lengths ( $d_{\text{Bi-Te}}$ ) close to that of coordination C.

infers a sizable variation of the  $\alpha_R$  even in the same batch of  $\text{Cu}_x\text{BiTeI}$  crystals.

The Cu dopings are most likely achieved through the internal redox reaction of the intercalated Cu in the van der Waals gap. While there is no superlattice observed from both powder X-ray and Laue diffraction results up to about 20 % Cu intercalation per formula unit, the intercalated Cu should distribute randomly or in vari-

ous domain sizes within the van der Waals gap. Locally, the induced strain by Cu can be relieved by expanding the lattice along the stacking direction (the inset of Fig. 1(b)) and also by distorting both the  $d_{\text{Bi-Te}}$  and  $d_{\text{Bi-I}}$  in the same manner. It is then reasonable to describe the various degree of residue strain of a layered system with an average  $d_{\text{Bi-Te}}$  change. By assuming the change of  $d_{\text{Bi-I}}$  scales linearly with  $d_{\text{Bi-Te}}$  due to Cu intercalation, the calculated  $\alpha_R$  values along AL and AH directions can vary as much as 20 % (6 - 4.8 eV\AA) while  $d_{\text{Bi-Te(I)}}$  merely drops by 1 % (3.07 - 3.03 \AA) as demonstrated in Fig. 5(b), which suggests a nontrivial role of average  $d_{\text{Bi-Te}}$  in the observed Rashba spin splitting effect. In Table I, both the calculated  $F$  and  $m^*$  values for coordination C drop monotonically with decreasing electron density  $n_e$  while the ratio of  $A_L/A_S (= F_L/F_S)$  increases with descending  $n_e$ . Apparently, the experimental values in Table I gives a smaller  $F_L/F_S$  ratio at similar carrier densities that can not be fully explained by the discrepancy in  $n_e$ . We, therefore, attribute the likely source of deviation to the difference in average  $d_{\text{Bi-Te}}$  that dictates  $\alpha_R$ . Nevertheless, further investigation is keenly required to show how does  $d_{\text{Bi-Te(I)}}$  in BiTeI influence the charge distribution in  $(\text{BiTe})^+$  layer and hence the Rashba spin splitting effect.

In conclusion,  $\text{Cu}_x\text{BiTeI}$  is a remarkable system, where we have demonstrated a robust impact of a minor change in atomic coordinations to its band property. The Cu doping not only effectively reduces the electron density but also boosts the carriers' Hall mobility. We observed two distinct frequencies in SdH oscillation, where the corresponding effective cyclotron masses were determined and compared to theoretical band calculations using three different atomic coordinations for Te and I. Our experimental data agree well with the calculation using coordination C with a shortest  $d_{\text{Bi-Te}}$ , which indicates a close connection between  $d_{\text{Bi-Te}}$  and the giant bulk Rashba spin splitting effect in BiTeI. In principle,  $\alpha_R$  can be readily tuned by controlling the BiTeI bond length if applicable. Our finding offers a new possibility for engineering the Rashba spin splitting in a layered and noncentrosymmetric material.

The authors acknowledge the funding support from National Science Council in Taiwan. W.L.L. acknowledges the funding support from Academia Sinica 2012 career development award in Taiwan.

\* Electronic address: wlee@phys.sinica.edu.tw

- [1] K. Ishizaka *et al.*, Nature Mater. **10**, 521 (2011)
- [2] S. V. Eremeev, I. A. Nechaev, Y. M. Koroteev, P. M. Echenique, and E. V. Chulkov, Phys. Rev. Lett. **108**, 246802 (2012)
- [3] M. Sakano *et al.*, Phys. Rev. Lett. **110**, 107204 (2013)

- [4] M. S. Bahramy, B. J. Yang, R. Arita and N. Nagaosa, Nature Commun. **3**, 679 (2011)
- [5] A. V. Shevelkov *et al.*, J. Solid State Chem. **114**, 397 (1995).
- [6] A. Crepaldi *et al.*, Phys. Rev. Lett. **109**, 096803 (2012)
- [7] J. S. Lee *et al.*, Phys. Rev. Lett. **107**, 117401 (2011)
- [8] G. Landolt *et al.*, Phys. Rev. Lett. **109**, 116403 (2012)
- [9] V. A. Kulbachinskii *et al.*, J. Solid State Chem. **193**, 154 (2012).
- [10] M. S. Bahramy, R. Arita, and N. Nagaosa, Phys. Rev. B **84**, 041202(R) (2011)
- [11] C. Martin, E. D. Mun, H. Berger, V. S. Zapf, and D. B. Tanner, Phys. Rev. B **87**, 041104(R) (2013)
- [12] C. Bell *et al.*, Phys. Rev. B **87**, 081109(R) (2013)
- [13] R. Sankar, W. L. Lee, and F. C. Chou, unpublished.
- [14] See supplementary materials at XXX for details of SdH oscillation analysis.
- [15] J. P. Perdew, K. Burke and M. Ernzerhof, Phys. Rev. Lett. **77**, 3865 (1996)
- [16] G. Kresse and J. Hafner, Phys. Rev. B **48**, 13115 (1993)
- [17] G. Kresse and J. Furthmüller, Comput. Mater. Sci. **6**, 15 (1993)
- [18] We have also determined the Te and I atomic positions theoretically by fully relativistic GGA[15] calculations using the PAW method[16, 17]. Our theoretical atomic positions of Te(2/3,1/3,0.7458) and I(1/3,2/3,0.3133) are nearly identical to that reported in [10] (the bond length differences being within 1.0 %).